Preprints of the 19th World Congress
The International Federation of Automatic Control
Cape Town, South Africa. August 24-29, 2014

Nonlinear Dynamics of Hysteresis-Based Load Controls ⋆

Soumya Kundu * **Ian A. Hiskens** **

* *Center for Nonlinear Studies, Los Alamos National Laboratory, Los Alamos, NM 87545, USA*
** *Department of Electrical Engineering and Computer Science, University of Michigan, Ann Arbor, MI 48109, USA*

Abstract: Direct load control can be achieved by varying the hysteresis band of switchable loads, thereby changing their on/off durations. Such hysteresis-based control methods may, however, display complex dynamics that must be thoroughly understood in order to design safe control mechanisms. This paper explores the dynamical behavior of a group of hysteresis-based PEV chargers. Of interest is the change in the total power demand of the group as the hysteresis-band limits are varied. A detailed state-space model is used to capture the dynamics of the load aggregation. This model suggests that for certain control inputs, e.g. periodic ramp signals, the system may display rich dynamical behavior. It is observed that structural stability of the system may be disrupted as certain characteristics of the input signal are varied. The paper explores these phenomena through a bifurcation analysis of the load population dynamics. The results identify performance limitations that govern the responsiveness of fast-acting demand control.

Keywords: Load control, PEV charging, bifurcations.

1. INTRODUCTION

Electrical loads, when considered in aggregation, have the potential to provide useful demand-side control. However, because of their diversity and incoherent operations, it is challenging to derive models that can truly capture the population response. While a simplistic linearized response model can often be used for closed-loop demand control, it is nevertheless important to understand the complex population dynamics.

Loads that operate according to a hysteresis band, e.g. thermostatic loads, provide significant opportunities for non-disruptive control strategies. Load control is achieved by adjusting the hysteresis band of each participating load to effect a change in aggregate power demand. In Callaway (2009), such a control mechanism was proposed for thermostatically controlled loads, e.g. air conditioners and water heaters, based on a model developed using system identification techniques. Later in Callaway and Hiskens (2011), the authors showed that it is possible to devise a hysteresis-based charging protocol for plug-in electric vehicle (PEV) chargers. Several studies have considered the modeling and control of hysteresis-based loads, including Callaway and Hiskens (2011); Callaway (2009); Bashash and Fathy (2011); Koch et al. (2011); Mathieu and Callaway (2012); Perfumo et al. (2012); Kundu et al. (2011); Kundu and Hiskens (2012). Generally these models can predict the system output for certain restrictive control input signals. A more detailed state-space model developed in Kundu and Hiskens (2013) offers the possibility of capturing the aggregate response under a wider range of control inputs.

This paper presents results from a study of the nonlinear dynamical properties of a collection of hysteresis-based loads. Bifurcation diagram analysis is used to record the change in system behavior as a control parameter is varied, while time-domain waveforms from the model developed in Kundu and Hiskens (2013) are used to explore the response at some of the interesting parameter values. Section 2 briefly discusses a hysteresis-based charging mechanism for PEVs and presents a state-space model for aggregate demand response. Section 3 shows how this control can initiate nonlinear dynamic demand response. This behavior is investigated in Section 4, and conclusions are presented in Section 5.

2. SYSTEM MODEL

A large homogeneous group of PEV chargers (of population size N_v) is considered. The hysteresis-based charging mechanism used here was first proposed in Callaway and Hiskens (2011), and later studied for modeling and control purposes in Kundu and Hiskens (2012, 2013). While the focus here is on a group of PEV chargers, the concepts can be applied equally as well to any collection of loads that operate on a hysteresis band, e.g. thermostatic loads.

2.1 Hysteresis-based charging of PEVs

Hysteresis-based charging of PEVs follows an ON-OFF sequence, such that the state-of-charge of the PEV battery $SoC(t)$ always remains within a hysteresis band con-

⋆ Research supported by the National Science Foundation through EFRI-RESIN grant 0835995, and the Department of Energy through the Clean Energy Research Centre for Clean Vehicle Collaboration (CERC-CVC), award number DE-PI0000012.

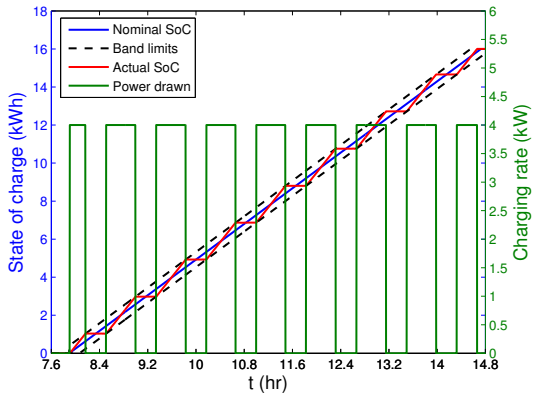

(a) Full charging period.

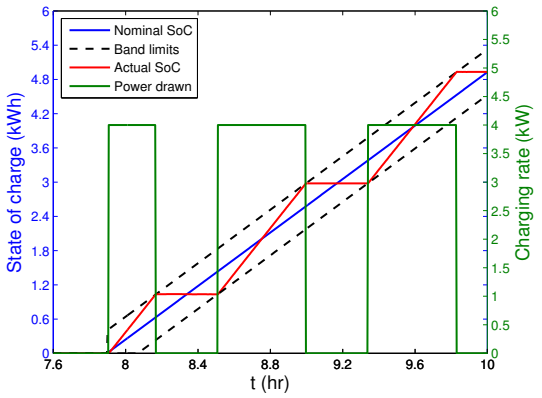

(b) Expanded view of the first few hours of charging.

Fig. 1. A typical hysteresis-based PEV charging profile.

Table 1. Key Symbols.

N_v	number of PEVs
N	number of bins across the hysteresis band
SoC	state-of-charge (SOC) (kWh)
SoC_{nom}	nominal SOC (kWh)
$\widetilde{SoC}$	normalized SOC
P_{max}	maximum charging rate (kW)
P_{nom}	nominal charging rate (kW)
P_{tot}	total demand of the PEV population (MW)
E_{max}	battery charge capacity (kWh)
Δ	normalized hysteresis-band width
α_{on}	rate of increase of normalized SOC (min^{-1})
α_{off}	rate of decrease of normalized SOC (min^{-1})
$x_i(t)$	probability density of chargers in i-th bin
δ_{bin}	width of each bin in the hysteresis band
$u(t)$	shift in normalized SOC profile over time
$v(t)$	rate of change $v(t) = du(t)/dt$ (min^{-1})
T_u	time period of the control input (min)

structed evenly around a "nominal" state-of-charge profile $SoC_{nom}(t)$, as shown in Fig. 1. The nominal state-of-charge profile could be a simple linearly increasing profile from zero to the maximum charge requirement E_{max}, which is the case in Fig. 1, or one that is beneficial for the grid, e.g. overnight "valley" filling, see Kundu and Hiskens (2012). Based on the nominal state-of-charge $SoC_{nom}(t)$, the "nominal" charging rate can be defined as $P_{nom}(t) := \frac{d}{dt} SoC_{nom}(t)$. In the sequel, it will be assumed for convenience that the nominal state-of-charge is linearly increasing, and hence the nominal charge rate is constant over time, i.e. $P_{nom}(t) = P_{nom}$. This is not a restrictive assumption though.

Defining the normalized state-of-charge by,

$$\widetilde{SoC}(t) := \frac{SoC(t) - SoC_{nom}(t)}{E_{max}}, \tag{1}$$

the resulting charging dynamics can be expressed as,

$$\dot{\widetilde{SoC}}(t) = \frac{s(t)P_{max} - P_{nom}}{E_{max}} \tag{2a}$$

where $\dot{s} = 0$ except at reset events,

$$s(t^+) = \begin{cases} s(t)+1 & \text{when } s(t) = 0 \wedge \widetilde{SoC} = -\Delta/2 \\ s(t)-1 & \text{when } s(t) = 1 \wedge \widetilde{SoC} = \Delta/2, \end{cases} \tag{2b}$$

with t^+ denoting the time instant immediately following the switching event. The width of the normalized hysteresis band is Δ.

The remainder of the paper considers the normalized hysteresis band and normalized state-of-charge, so the term "normalized" will be dropped for simplicity. Moreover, define:

$$\alpha_{on} := \frac{P_{max} - P_{nom}}{E_{max}} \tag{3a}$$

$$\alpha_{off} := -\frac{P_{nom}}{E_{max}}, \tag{3b}$$

as the rate of increase and decrease, respectively, of normalized state-of-charge. These quantities will be referred to henceforth as the "natural rates".

2.2 Control action

The aggregate power demand of a collection of hysteresis-based devices can be controlled by adjusting the limits of the hysteresis band, while maintaining a constant hysteresis-band width Δ. Moving the hysteresis band in the direction of the limit associated with ON-to-OFF switching increases the overall demand by delaying ON-to-OFF switching and inducing premature OFF-to-ON switching. Likewise, a decrease in the overall demand can be achieved by moving the hysteresis band in the opposite direction. A more complete discussion is provided by Callaway (2009).

Let the rate at which control action shifts the hysteresis-band limits be given by $v(t) \in \mathbb{R}$. Consequently, variation in the position of the hysteresis-band limits is given by,

$$u(t) = \int_0^t v(\tau) d\tau. \tag{4}$$

Under this control action, the dynamic behavior of (2) becomes,

$$\dot{\widetilde{SoC}}(t) = \begin{cases} \alpha_{on}, & s(t) = 1 \\ \alpha_{off}, & s(t) = 0 \end{cases} \tag{5a}$$

where $\dot{s} = 0$ except at reset events

$$s(t^+) = \begin{cases} s(t)+1 & \text{when } s(t) = 0 \wedge \widetilde{SoC} = -\Delta/2 + u(t) \\ s(t)-1 & \text{when } s(t) = 1 \wedge \widetilde{SoC} = \Delta/2 + u(t). \end{cases} \tag{5b}$$

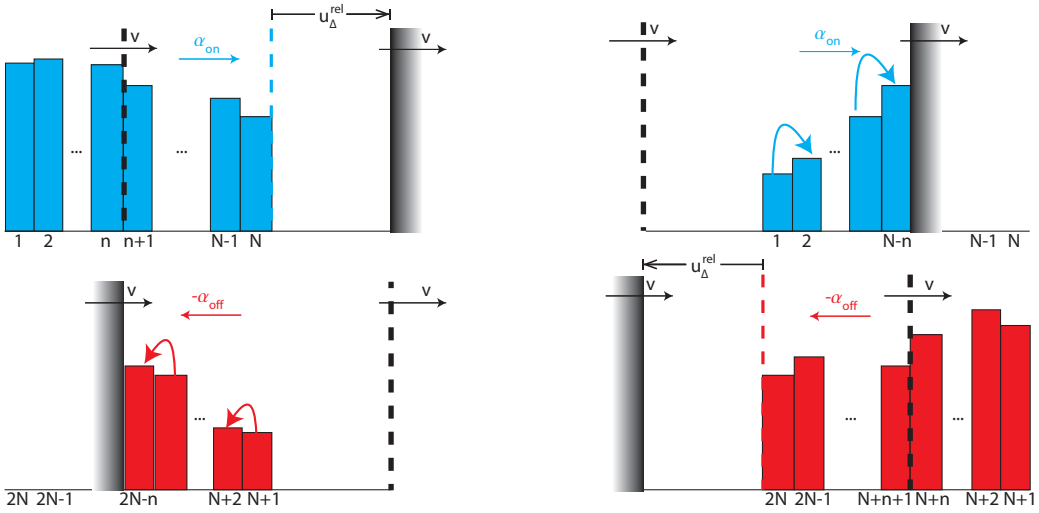

(a) Chargers lie to the left of the lower hysteresis-band limit.

(b) Chargers lie to the right of the upper hysteresis-band limit.

Fig. 2. Inter-bin migration when the hysteresis band moves with rate $v(t)$ under control action. (In both figures, the upper half of the bins correspond to the ON-state chargers, while the lower half correspond to the OFF state.)

2.3 State-space model

The desired state-space model must be able to capture the changes in the aggregate power demand of the PEV population in response to the control action $v(t)$. One modeling approach, previously used in the context of thermostatic loads, is to divide the probability distribution of the population's state-of-charge into several bins. The probability density associated with each of those bins is then evaluated as the state-of-charge of individual PEVs evolves according to (5). Further details can be found in Koch et al. (2011); Bashash and Fathy (2011); Mathieu and Callaway (2012).

Accordingly, the width of the hysteresis band Δ is divided into N bins, each having equal width $\delta_{bin} = \Delta/N$. A state-space of size $2N$ is constructed, $[x_1(t), x_2(t), \ldots, x_{2N}(t)]$, where the first N states represent the probability densities of the ON-state bins, while the last N represent the OFF-state bins. The total power demand is given by,

$$P_{tot}(t) = N_v P_{max} \delta_{bin} \sum_{i=1}^{N} x_i(t). \tag{6}$$

To keep track of the position of the bins with respect to the moving hysteresis band, Kundu and Hiskens (2013) introduced a variable $u_\Delta^{rel}(t)$ that describes the distance between the hysteresis band and the population bins, as illustrated in Fig. 2. The behavior of $u_\Delta^{rel}(t)$ is given by,

$$\frac{du_\Delta^{rel}(t)}{dt} = y(t) \tag{7a}$$

where,

$$y(t) = \begin{cases} v(t) - \alpha_{on}, & \left(u_\Delta^{rel}(t) = 0 \wedge v(t) \geq \alpha_{on}\right) \vee u_\Delta^{rel}(t) > 0 \\ v(t) - \alpha_{off}, & \left(u_\Delta^{rel}(t) = 0 \wedge v(t) \leq \alpha_{off}\right) \vee u_\Delta^{rel}(t) < 0 \\ 0, & \text{otherwise.} \end{cases} \tag{7b}$$

When all the chargers lie within the hysteresis-band limits, $u_\Delta^{rel}(t) = 0$. With $u_\Delta^{rel}(t) > 0$, some or all chargers lie to the left of the lower band limit, as shown in Fig. 2(a). When $u_\Delta^{rel}(t) < 0$, chargers lie to the right of the upper band limit, as shown in Fig. 2(b). The number of bins n_t lying outside the hysteresis band, at time t, can be expressed as,

$$n_t = \min\left(\left\lceil \frac{|u_\Delta^{rel}(t)|}{\delta_{bin}} \right\rceil, N\right) \tag{8}$$

where the 'ceiling' function is used to convert the fraction into an integer.

In the case when all the chargers lie inside the hysteresis band, $u_\Delta^{rel}(t) = 0$, and the band moves more slowly than the 'natural' rates, $\alpha_{off} < v(t) < \alpha_{on}$, the equations governing state dynamic behavior can be written,

$$\dot{x}_i(t)\delta_{bin} = \begin{cases} -x_{2N}(\alpha_{off} - v) - x_1(\alpha_{on} - v), & i = 1 \\ (x_{i-1} - x_i)(\alpha_{on} - v), & i = 2, ..., N \\ x_N(\alpha_{on} - v) + x_{N+1}(\alpha_{off} - v), & i = N+1 \\ -(x_{i-1} - x_i)(\alpha_{off} - v), & i = N+2, ..., 2N. \end{cases} \tag{9}$$

If the control input varies faster than the natural rates, some or all of the chargers will fall outside the hysteresis band. This situation corresponds to $u_\Delta^{rel}(t) \neq 0$. When $u_\Delta^{rel}(t) > 0$, the state-space equations governing behavior become,

$$\dot{x}_i(t)\delta_{bin} = \begin{cases} x_{2N-n_t} \max\big(0, v - \alpha_{off}\big), & i = n_t + 1 \\ x_i(\alpha_{off} - \alpha_{on}), & i = N+1 \\ -\big(x_{i-1} - x_i\big)(\alpha_{off} - \alpha_{on}), & i = N+2, .., 2N - n_t - 1 \\ -x_i \max\big(0, v - \alpha_{off}\big) & \\ \quad - x_{i-1}(\alpha_{off} - \alpha_{on}), & i = 2N - n_t \\ 0, & \text{all other } i \end{cases} \tag{10}$$

while the state equations applicable when $u_\Delta^{rel}(t) < 0$ are,

$$\dot{x}_i(t)\delta_{bin} = \begin{cases} -x_i(\alpha_{on}-\alpha_{off}), & i=1 \\ \big(x_{i-1}-x_i\big)(\alpha_{on}-\alpha_{off}), & i=2,\ldots,N-n_t-1 \\ -x_i \max\big(0,\alpha_{on}-v\big) & \\ \qquad + x_{i-1}(\alpha_{on}-\alpha_{off}), & i=N-n_t \\ x_{N-n_t}\max\big(0,\alpha_{on}-v\big), & i=N+n_t+1 \\ 0, & \text{all other } i. \end{cases} \tag{11}$$

In subsequent investigations [1], the response of this model is compared with a Monte-Carlo simulation where 2000 PEVs were simulated using the dynamic model (5).

3. NONLINEAR DYNAMIC BEHAVIOR

The switching behavior inherent in hysteresis-based loads, when aggregated over a large population, can result in nonlinear synchronizing effects. Consider a control input $u(t)$, i.e. the shift from the nominal hysteresis band, which ramps up and down periodically. Such an input signal is shown in Fig. 3(a). In this initial case, the input varies more slowly than the "natural" rates, as shown in Fig. 3(b), so the chargers always stay within their hysteresis band. Accordingly, $u_{\Delta}^{rel}(t)$ remains zero throughout. Each ramp-up and ramp-down sequence has the same duration of 15.4 min. The resulting demand response is a period-1 waveform which oscillates between the maximum demand of $N_v \times P_{max} = 8$ MW and zero, see Fig. 3(c).

Interesting behavior can be observed, however, as the control-input period is gradually decreased. Fig. 4 shows one such scenario where the total period of the input is reduced to 24.4 min, while keeping the ramp rates unchanged. Aggregate demand, shown in Fig. 4(c), exhibits a period-2 orbit, i.e. has a period twice that of the input, and experiences a reduction in amplitude.

To ensure this nonlinear behavior was not an artifact of the state-space model, Monte-Carlo simulation results were compared with the state-space model. Figs. 3(c) and 4(c) show that both forms of modeling produce almost exactly the same response.

This behavior was further investigated by plotting a bifurcation diagram using Monte-Carlo simulation. The period of the input T_u was varied over a wide range while keeping other parameters fixed. The intersections of the output (aggregate PEV charging demand P_{tot}) with a Poincaré plane given by

$$P_n := P_{tot}\left(nT_u\right), \quad n \in \mathbb{N}, \tag{12}$$

were plotted. To remove the effects of transients, only the intersection points for $n > 5$ were used. The resulting bifurcation diagram is shown in Fig. 5. For values of the period $T_u > 30$ min, the demand follows a period-1 orbit. Periodicity collapses as T_u is reduced though, until a period-2 orbit appears at about 26 min. That periodicity again collapses as T_u is reduced to around 23 min. Continuing this process of decreasing T_u produces a period-adding cascade, with successive periodic regions interspersed by regions of aperiodicity.

[1] The system parameters are: $N_v = 2000$, $\Delta = 0.05$, $P_{max} = 4$ kW, $P_{nom} = 2.4$ kW, $E_{max} = 16$ kWh. The continuous dynamics in (5) was discretized using a time step of 0.2 min.

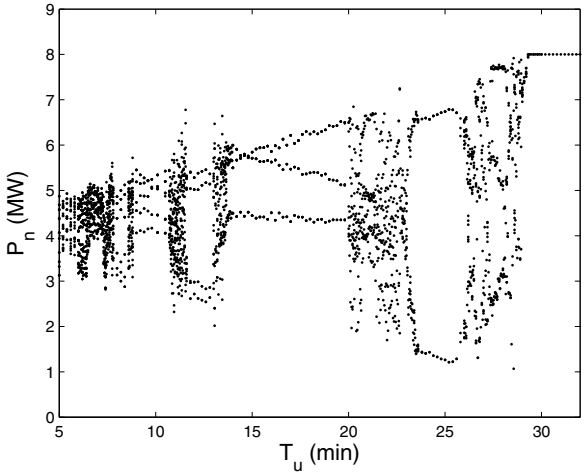

Fig. 5. Bifurcation diagram when the input is a periodic ramp, with ramp-up and ramp-down rates of 0.0013 min^{-1} and 0.0017 min^{-1}, respectively.

4. CRITICAL OBSERVATIONS

4.1 Variations in behavior

It is interesting to consider the emergence of other nonlinear behavior as the input period is varied over a wider range. Figs. 6(a) and 6(b) show the existence of other period orbits. These two scenarios correspond to T_u values of 15.6 min and 12.4 min, and display period-3 and period-4 orbits, respectively. Note that the ramp rates remain unchanged from their previous values.

Figs. 6(a) and 6(b) indicate that the state-space model of Section 2.3 is able to capture the higher periodic behavior with good accuracy. However, model accuracy reduces dramatically when the period is chosen from within one of the aperiodic regions. Referring to Fig. 5, the period $T_u =$ 28.8 min lies in such a region. Fig. 6(c) shows behavior in this case. The state-space model and the Monte-Carlo simulation are initially quite close, but deviate from each other after about one input cycle. This suggests chaotic behavior, where a small error in the initial conditions can quickly grow. Further analysis is required to fully understand this breakdown in periodicity.

4.2 Faster ramp rates

To investigate the bifurcations induced for other ramp rates, the nonlinear behavior of the aggregate demand was studied for ramp rates that were faster than the natural rates. A comparison between Monte-Carlo simulation and the state-space model, under these more onerous conditions, was also undertaken.

Fig. 7 shows a bifurcation diagram when the ramp rates were chosen from beyond the natural rates, α_{on} and α_{off}. It can be seen that the stable range for the period-1 orbit extends down to $T_u \approx 24$ min. Moreover the period-2 orbit observed in Fig. 5 has disappeared. As T_u decreases, a

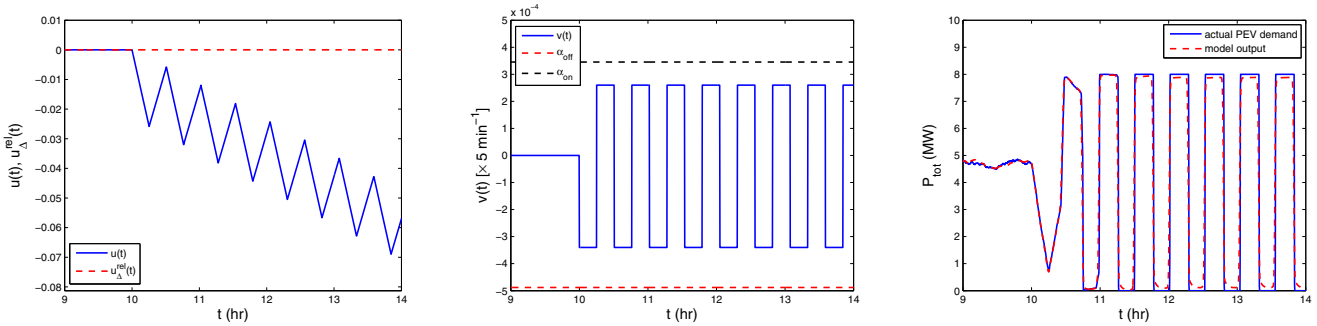

(a) Shift $u(t)$ in hysteresis band. (b) Hysteresis-band shift rate $v(t)$. (c) Controlled output, total demand P_{tot}.

Fig. 3. Period-1 response to an input of equal-width ramp-up and ramp-down sequences with rates of 0.0013 min^{-1} and 0.0017 min^{-1}, respectively, and a period of $T_u = 30.8$ min.

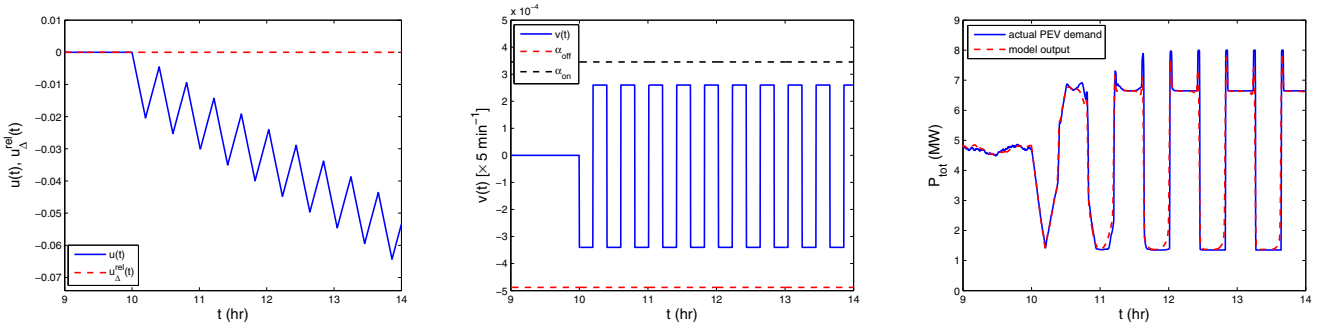

(a) Shift $u(t)$ in hysteresis band. (b) Hysteresis-band shift rate $v(t)$. (c) Controlled output, total demand P_{tot}.

Fig. 4. Period-2 response to an input of equal-width ramp-up and ramp-down sequences with rates of 0.0013 min^{-1} and 0.0017 min^{-1}, respectively, and a period of $T_u = 24.4$ min.

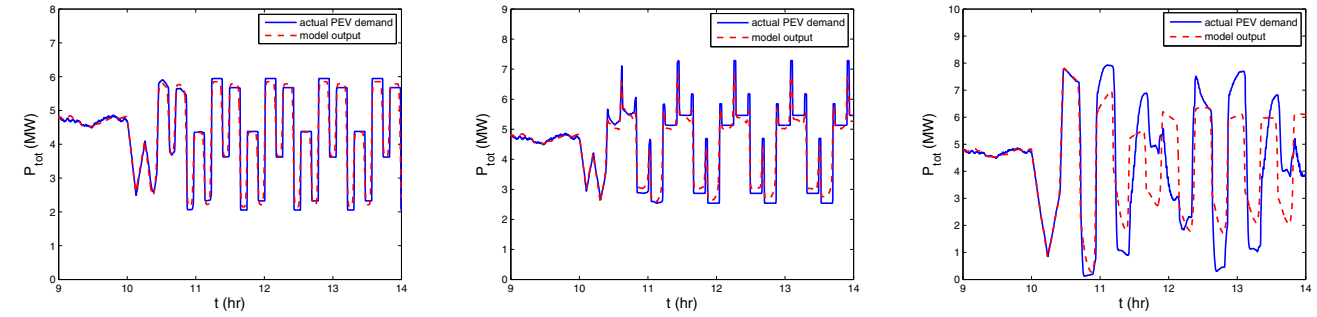

(a) Period $T_u = 15.6$ min. (b) Period $T_u = 12.4$ min. (c) Period $T_u = 28.8$ min.

Fig. 6. Demand response at different values of period T_u, with the ramp-up and ramp-down rates fixed at 0.0013 min^{-1} and 0.0017 min^{-1}, respectively.

period-3 orbit closely follows the period-1 orbit, after a narrow band of aperiodicity. Subsequently period-5 orbits exist, followed by another band of aperiodicity, with no discernible existence of period-4 orbits. Fig. 8 confirms the existence of a period-1 orbit at $T_u = 24.4$ min. Because the ramp rates are higher (in magnitude) than the natural rates, as shown in Fig. 8(b), some chargers fall outside the hysteresis band, giving rise to non-zero values of $u_\Delta^{rel}(t)$, as shown in Fig. 8(a).

Although Fig. 7 suggests that very narrow bands of period-2 and period-4 orbits are present at T_u values around 13 min and 9.5 min, respectively, the time-domain waveforms in Figs. 9(a) and 9(c) indicate otherwise. Fig. 9(b) shows the presence of an aperiodic region between the stable period-3 and period-5 regions.

It can be observed from the bifurcation analysis of Fig. 7 that for faster ramp rates, the period-1 orbit is stable for a larger parameter region, and period-2 and period-4 orbits appear to be absent (or almost indiscernible). In preliminary analysis, these two findings seem to be quite general for input ramp rates that are faster than the natural rates. Fig. 10 provides a bifurcation diagram for ramp-up and ramp-down rates of 0.003 min^{-1} and 0.004 min^{-1}, respectively. The period-1 orbit now extends down to $T_u = 20$ min, followed by a narrow band of

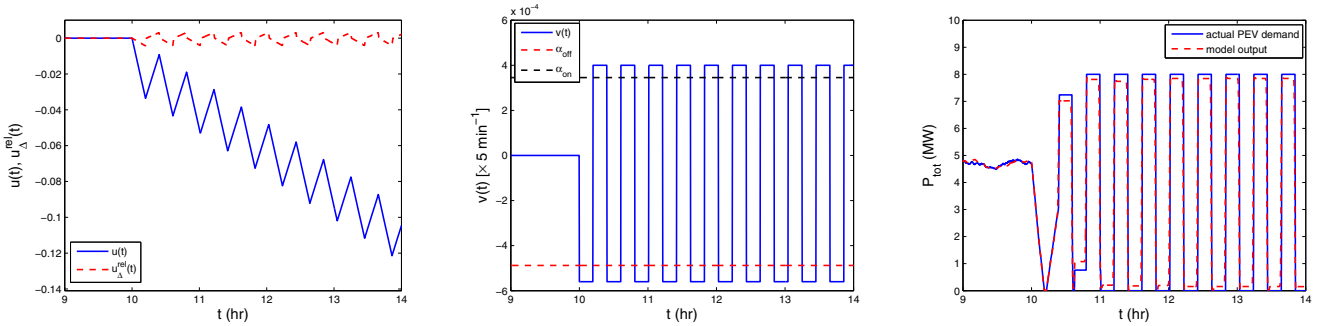

(a) Shift $u(t)$ in hysteresis band, with non-zero u_{Δ}^{rel}.

(b) Hysteresis-band shift rate $v(t)$.

(c) Controlled output, total demand P_{tot}.

Fig. 8. Period-1 response for input period, $T_u = 24.4$ min, and ramp-up and ramp-down rates of 0.002 min^{-1} and 0.0028 min^{-1}, respectively.

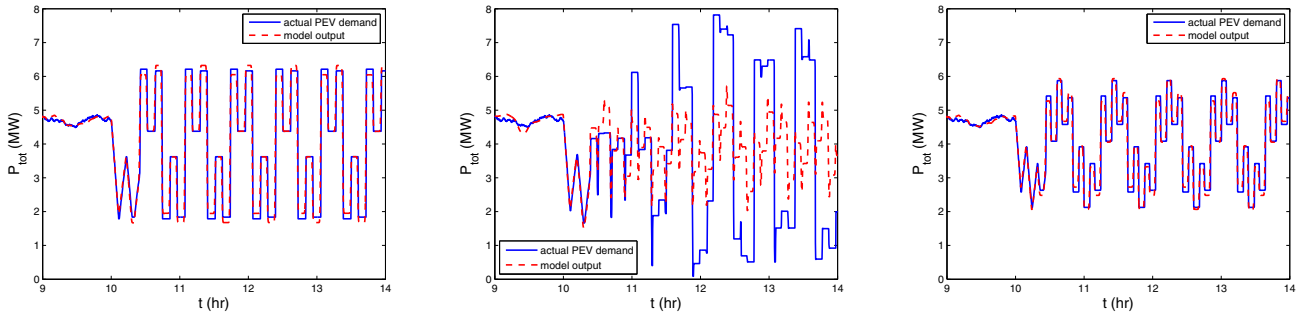

(a) At T_u =13.2 min

(b) At T_u =11.93 min

(c) At T_u =9.6 min

Fig. 9. Demand response at different values of period T_u, with the ramp-up and ramp-down rates fixed at 0.002 min^{-1} and 0.0028 min^{-1}, respectively.

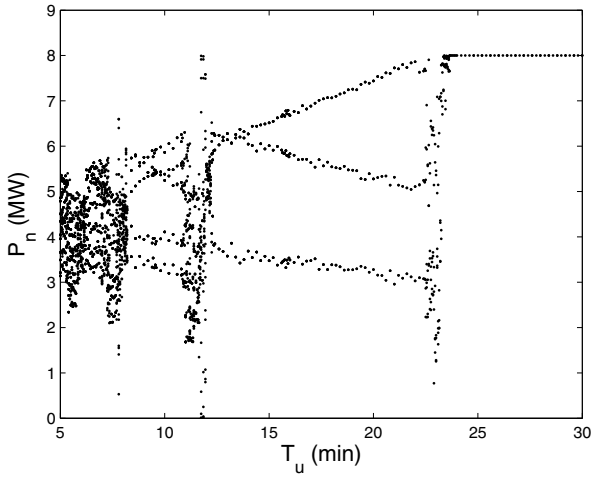

Fig. 7. Bifurcation diagram when the input is a periodic ramp, with ramp-up and ramp-down rates of 0.002 min^{-1} and 0.0028 min^{-1}, respectively.

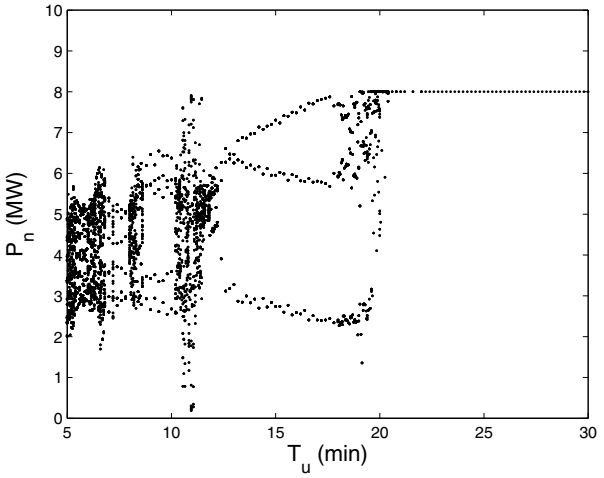

Fig. 10. Bifurcation diagram when the input is a periodic ramp, with ramp-up and ramp-down rates of 0.003 min^{-1} and 0.004 min^{-1}, respectively.

aperiodicity and then a region of period-3 orbits. The period-2 and period-4 orbits have disappeared.

5. CONCLUSIONS

The work presented here shows that hysteresis-based control of electrical loads may exhibit rich dynamical behavior. It has been observed that structural stability of the system can be disrupted by changing crucial parameters. Bifurcation diagrams have been obtained by varying the period of a periodic ramp input. A period adding cascade was observed with ramp rates slower than the natural rates. Robustness of the period-1 orbit was found to increase when the ramp rates were faster than the natu-

ral rates. Furthermore, it was shown that such complex nonlinear behavior can be reproduced using a state-space model. This model appears promising for future investigations into the dynamics of hysteresis-based load control schemes. This will be vital for designing effective demand control algorithms.

REFERENCES

Bashash, S. and Fathy, H. (2011). Modeling and control insights into demand-side energy management through setpoint control of thermostatic loads. In *Proceedings of the American Control Conference*, 4546–4553. San Francisco, CA.

Callaway, D. (2009). Tapping the energy storage potential in electric loads to deliver load following and regulation, with application to wind energy. *Energy Conversion and Management*, 50, 1389–1400.

Callaway, D. and Hiskens, I. (2011). Achieving controllability of electric loads. *Proceedings of the IEEE*, 99(1), 184–199.

Koch, S., Mathieu, J., and Callaway, D. (2011). Modeling and control of aggregated heterogeneous thermostatically controlled loads for ancillary services. In *Proceedings of the 17th Power Systems Computations Conference*. Stockholm, Sweden.

Kundu, S. and Hiskens, I. (2012). Hysteresis-based charging control of plug-in electric vehicles. In *Proceedings of the 51st IEEE Conference on Decision and Control*, 5598–5604. Maui, HI.

Kundu, S. and Hiskens, I. (2013). State-space modeling of hysteresis-based control schemes. In *Proceedings of the 12th European Control Conference*. Zurich, Switzerland.

Kundu, S., Sinitsyn, N., Backhaus, S., and Hiskens, I. (2011). Modeling and control of thermostatically-controlled-loads. In *Proceedings of the 17th Power Systems Computations Conference*. Stockholm, Sweden.

Mathieu, J. and Callaway, D. (2012). State estimation and control of heterogeneous thermostatically controlled loads for load following. In *Proceedings of the 45th Hawaii International Conference on System Sciences*, 2002–2011.

Perfumo, C., Kofman, E., Braslavsky, J., and Ward, J. (2012). Load management: Model-based control of aggregate power for populations of thermostatcally controlled loads. *Energy Conversion and Management*, 55, 36–48.